Received: 18 February 2026 | Revised: 3 May 2026 | Accepted: 5 May 2026

DOI: 10.1002/prs.70066

PROCESS SAFETY PROGRESS

ORIGINAL ARTICLE

Impact of metal corrosion on the process safety of foam fire suppression system

Kai Wang[1,2] | Qihang Yue[1,2] | Peiyao Chen[3] | Xikang Zhang[2] | Lichen Zhang[3] | Zhengyang Wang[4] | Wei Wang[4] | Liming Hu[5] | Biao Zhou[1,2]

[1]Inner Mongolia Research Institute, China University of Mining and Technology (Beijing), Ordos, China

[2]School of Emergency Management and Safety Engineering, China University of Mining and Technology (Beijing), Beijing, China

[3]Tianjin Fire Research Institute of Ministry, Ministry of Emergency Management, Tianjin, China

[4]Shanghai Fire Research Institute of Ministry, Ministry of Emergency Management, Shanghai, China

[5]Safety Department, China Energy Engineering Group Corporation Limited, Beijing, China

Correspondence
Biao Zhou, Inner Mongolia Research Institute, China University of Mining and Technology (Beijing), Ordos 017010, China.
Email: zhoubiao1088@cumtb.edu.cn

Funding information
Ordos Key Research and Development Program, Grant/Award Number: YF20240026; Beijing Nova Program, Grant/Award Number: 202504841008; Key-Area Research and Development Program of Guangdong Province, Grant/Award Number: 2024B1111080002; Fundamental Research Funds for the Central Universities, Grant/Award Number: 2025ZKPYAQ03; Natural Science Foundation of Shanghai, Grant/Award Numbers: 24ZR1473000, 25ZR1402516; Key Science and Technology Program of the MEM, Grant/Award Number: 2025EMST110301

Abstract

The long-term storage of foam extinguishing agent may lead to metal corrosion, which poses substantial risks to the safety and operational reliability of fire suppression systems. This study systematically investigated the performance evolution of foam extinguishing agent interacting with aluminum alloys through accelerated aging tests under elevated temperatures. The results showed that the aluminum alloy surface underwent significant corrosion. Meanwhile, the expansion ratio of the foam decreased by 37.46% and 12.84%, accompanied by precipitation and gelation. Molecular dynamics simulation revealed the mechanism by which aluminum ions coordinate and bridge with xanthan gum through electrostatic interactions, leading to foam concentrate changes. Fire suppression tests demonstrated that prolonged contact between the foam extinguishing agent and metal materials leads to performance deterioration. Moreover, the aged extinguishing agent exhibited poor miscibility with water during discharge, thereby hindering the effective progression of the fire suppression process. The findings highlight the critical importance of compatibility between foam agent and metallic material in process safety management. These results provide a scientific basis for the full life-cycle management of foam extinguishing agent and the maintenance of system reliability.

KEYWORDS
foam fire suppression system, metal corrosion, process safety, storage stability, system reliability

1 | INTRODUCTION

Aqueous film-forming foam (AFFF) has been widely applied across various industries due to its unique aqueous film-forming characteristic.[1–3] However, when applied to polar fuel surfaces, AFFF dissolves immediately.[4] By adding polysaccharide macromolecular compounds such as xanthan gum (XG) to the ordinary foam concentrate, the dehydration effect can be effectively reduced, forming an alcohol-resistant aqueous film-forming foam (AFFF/AR).[5–7]

Foam extinguishing agents are widely used in both indoor and outdoor environments, playing a critical role in fire suppression. Consequently, the integrity of storage vessels and the effectiveness of the agents are critical for proper maintenance and system reliability. A loss of concentrate quality or discharge capability is therefore not only a maintenance issue, but also a process safety issue. The storage

containers usually include fixed tank type and portable extinguishers, with materials commonly being carbon steel or aluminum alloy. To prevent chemical interactions between the agents and container materials, stringent design requirements have been established in various national standards. According to the Chinese standard "Technical standard for foam extinguishing systems" GB50151-2021, foam concentrate can corrode carbon steel and other metallic materials, thereby affecting the foam performance. Therefore, it is necessary to choose the appropriate material or corrosion-resistant coating. Similarly, the NFPA 11-2024 standard requires that the pipes, valves, and other components of foam fire extinguishing systems should all be made of suitable materials or coated with standard specifications of coatings.[8,9] However, due to cost constraints, some storage containers exhibit insufficient coating thickness, poor coating performance, or even the absence of protective coatings. In addition, because the inner surfaces of storage tanks are difficult to inspect, direct contact between the foam concentrate and the metal container is not uncommon. Such contact can lead to continuous corrosion of the container and chemical contamination of the foam concentrate. Consequently, these degradation effects significantly reduce the reliability of fire protection systems and increase the risk of system failure during fire emergencies.

Existing studies have indicated that corrosion is one of the primary factors threatening the reliability of fire protection systems.[10,11] There has been considerable research on metal corrosion in foam solutions. In these studies, the corrosion behavior of the alloys was mainly characterized using weight-loss immersion tests, electrochemical polarization measurements, and scanning electron microscopy. Previous studies have shown that the corrosion patterns of different metals vary depending on the type of foam solution. The corrosion rate in foam solutions is initially high but tends to stabilize over time, with the rate significantly increasing under high temperatures.[12,13] The protein and inorganic salt components in foam solutions promote the corrosion process, ultimately forming a porous cover with no protective effect.[8] Solvents such as hydrolyzed proteins, $FeSO_4$, urea, and ethylene glycol can exacerbate corrosion on alloys by promoting cathodic hydrogen evolution reactions and anodic metal dissolution reactions.[14,15] In summary, these studies have mainly focused on the corrosive effects of foam solutions on metal, while the contamination of foam solutions by metal has received less attention. The influence of corrosion-released metal ions on the performance of foam solutions remains poorly understood. Therefore, further investigation is needed to evaluate the continued usability of the affected solutions.

This study designed a high-temperature accelerated aging experiment to simulate the long-term storage condition in which foam concentrate remains in contact with aluminum alloy container. Key parameters such as surface tension and viscosity were systematically evaluated. Molecular dynamics simulation was conducted to elucidate the coupling mechanism between polysaccharide macromolecules and metal ions. The findings underscore the critical role of compatibility between foam agents and metallic materials in process safety management and provide a scientific basis for full life-cycle management, maintenance of system reliability, and evaluation of the actual performance of aged foam concentrate.

2 | MATERIALS AND METHODS

2.1 | Preparation of the concentrate

The formulations were prepared with the short-chain fluorocarbon surfactants Capstone™ 1157 and Capstone™ 1470 to lower surface tension, while sodium dodecyl sulfate and alkyl polyglucoside were used as hydrocarbon surfactants to improve foamability. And XG was then added as a foam stabilizer. The specific compositions are shown in Table 1. In order to reduce the error in the experiment, the concentrates were uniformly prepared and then divided into portions. When one bottle is removed during a certain cycle, it will not affect the aging process of the other concentrates.

2.2 | Accelerated aging test Methods

Under actual conditions, aging corrosion usually takes several years. According to the Chinese national standard GB 15308, the prescribed storage period is 2 years for AFFF/AR and extinguishing agents used in fire extinguishers. Products exceeding the prescribed storage period should undergo annual fire-extinguishing performance tests to determine whether they remain effective. In practice, foam concentrates stored beyond the prescribed shelf life are more likely to exhibit undesirable phenomena such as corrosion-related deterioration and performance degradation. Therefore, in this study, "long-term storage" refers to storage beyond the prescribed shelf life. The paper designs a thermal aging experiment at elevated temperature based on the time–temperature equivalence principle to rapidly achieve the aging effect equivalent to several years. Elevated temperature enhances molecular mobility and increases the rates of relevant reactions and mass transport processes, thereby reproducing the changes associated with long term storage within a short period.

After preparing the foam concentrates at specified ratios, aluminum alloy plates of identical dimensions were added to each sample, which were then sealed. The alloy plates consisted of aluminum as the base element (content >90%) with primary alloying elements including

TABLE 1 The formula of the foam concentrate.

Agent	Function	Mass fraction (%)
1157	Fluorocarbon surfactant	2.5
1470		2.5
SDS	Hydrocarbon surfactant	0.5
APG		4
Urea	Dispersant	5.7
Ethylene glycol	Antifreeze	1.5
Butyl diglycol	Co-solvent	10
Xanthan gum	Foam stabilizer	0/1.2
Water	Solvent	73.3/72.1
Total		100

silicon, copper, magnesium, manganese, and zinc. Subsequently, the labeled and sealed samples were placed in a constant temperature environmental chamber set at 80°C for continuous thermal aging. Samples were individually removed at aging periods of 8, 16, 32, 48, and 64 days. The experimental instruments are shown in Figure 1. After removal from the aging chamber, each sample was allowed to cool to room temperature before testing, which minimized the influence of residual heat on the measurements.

FIGURE 1 Environmental temperature test chamber.

2.3 | Testing methods

According to national regulatory standards, this study systematically tested the physicochemical properties of foam concentrates and their foam performance. The pH value and conductivity of foam concentrates were measured using a standard benchtop pH meter and conductivity meter. Viscosity measurements were conducted using a rotational viscometer to comprehensively evaluate the rheological characteristics of foam concentrates. Surface tension was tested using a Sigma 700 surface tensiometer on foam aqueous solutions. All tests were repeated three times and averaged to improve the stability and reliability of results. To further evaluate the foam performance, the foam expansion ratio was determined in accordance with the Chinese national standard GB 15308. A container with a fixed volume of 1335 mL was filled with foam, and the expansion ratio was calculated following the standard procedure. The drainage time was measured using standard drainage equipment, and the time required for 25% drainage was recorded with a stopwatch to assess foam stability. The fire extinguishing test device is shown in Figure 2. During the test, the prepared foam solution was charged into the system, and the gas cylinder was opened to establish the required driving pressure, while the discharge flow rate was regulated by a solenoid valve. Ethanol and gasoline pool fires were employed for AFFF/AR and AFFF. After a pre-burn period of 1 min, the foam was applied to the fuel surface by gentle application, and the extinguishing time was recorded.

2.4 | Molecular dynamics simulation configuration

In this work, two system boxes were constructed for experimental comparison: the AC1 box containing aluminum ions and the AC2

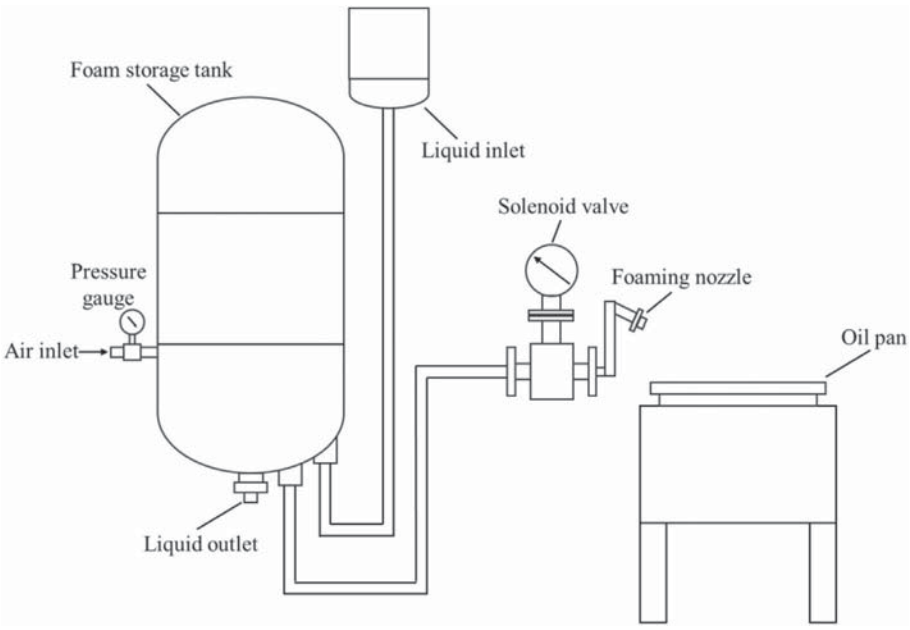

FIGURE 2 Foam fire extinguishing test device.

box without aluminum ions. Considering the mass fraction ratio between solvent and solute, the simulated AC1 box contained 4 XG particles with a degree of polymerization of 5 carrying 10 negative charges, 50 aluminum ions, and 5000 water molecules. The system was used to simulate the interaction between aluminum ions and XG under experimental conditions, with hydroxide ions added to the system to balance charges. In contrast, the AC2 box contained no aluminum ions as a control group, with hydronium ions added to balance charges, as shown in Figures 3 and 4.

The Forcite module in Materials Studio was employed to execute molecular dynamics simulation, with the PCFF force field selected to describe atomic interactions in the system. Prior to the dynamics simulation, each model underwent geometric optimization to achieve an energy-minimized equilibrium state. The total dynamics simulation time was set to 1 ns with a time step of 1.0 fs, employing an NVT ensemble with temperature control at 353 K using the Nose method. The Ewald method was selected for calculating electrostatic interaction summation, while the atom-based method was chosen for calculating van der Waals interaction summation. Here, NVT denotes the canonical ensemble, in which the number of particles, volume, and temperature remain constant during the simulation. And PCFF is a polymer consistent force field used to describe the interatomic interactions in the system.

3 | RESULTS AND DISCUSSION

3.1 | Appearance characteristics and precipitation behavior

The visual evolution of the aluminum surface is shown in Figure 5. A larger sample number indicates a longer aging time. As aging proceeds, the metallic luster of the aluminum surface diminishes markedly. In the AFFF system, corrosion traces initially appear mainly as dispersed discrete dots, and then develop into sheet-shaped corrosion features over a large area. After 64 days of aging, the coupon surface is clearly observed to be completely corroded. Meanwhile, as shown in Figure 6, the weight of the aluminum sheet progressively decreased during the early stage of aging but increased after 64 days. This trend indicates that the early stage is dominated by metal dissolution and mass loss. But in the later period, the deposition of corrosion products results in a mass gain. In the AFFF/AR system, localized corrosion features were also observed on the aluminum surface, as shown in Figure 5B, and the mass of the aluminum specimen initially decreased before gradually stabilizing.

When the concentrate serves as the ionic conduction path, the aluminum alloy undergoes electrochemical corrosion, and the corresponding cathodic reaction can be expressed as follows:

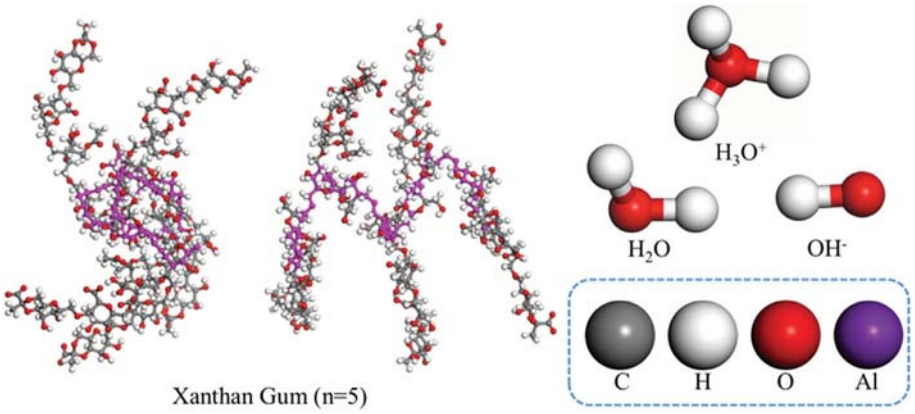

FIGURE 3 Particle configuration and corresponding elements.

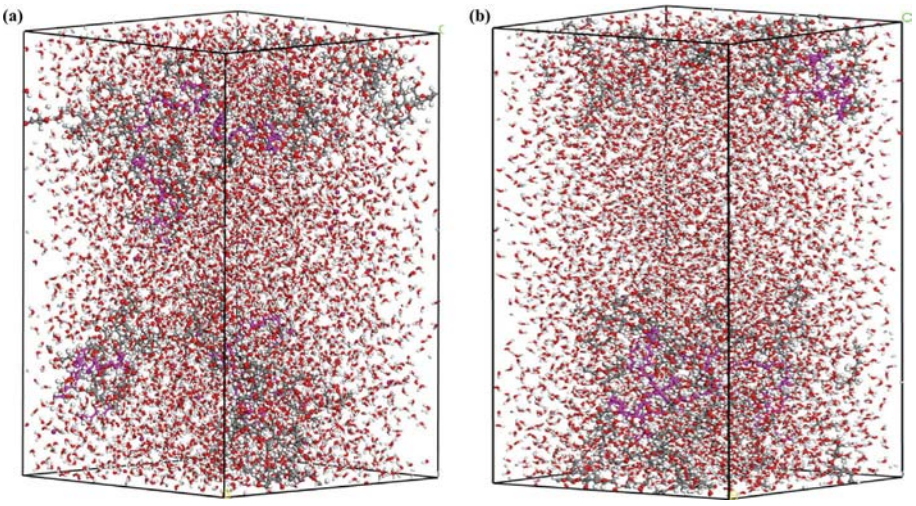

FIGURE 4 Simulation models of the samples: (A) AC1 (B) AC2.

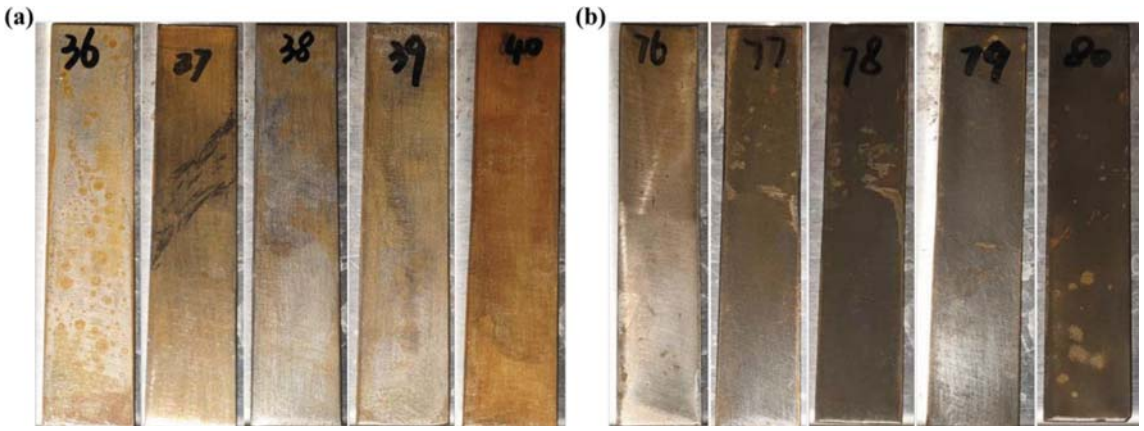

FIGURE 5 The diagram of aluminum alloy surface corrosion (A) AFFF (B) AFFF/AR.

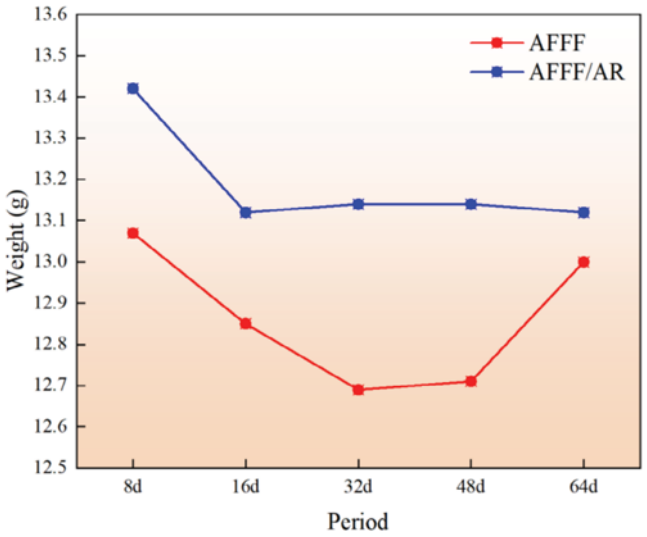

FIGURE 6 Mass change of the aluminum sheet during aging.

$$2H_2O + 2e^- \rightarrow H_2 + 2OH^- \quad (1)$$

At the anode, the aluminum alloy primarily experiences the oxidation of aluminum. Specifically, aluminum loses electrons to form Al^{3+}, and the generated aluminum ions subsequently react further with species in the concentrate.

$$Al \rightarrow Al^{3+} + 3e^- \quad (2)$$

Experimental results indicate that direct contact between the foam concentrate and the container accelerates corrosion. This not only compromises the continued serviceability of the storage container, but also reduces the operational reliability of the fire extinguishing system during emergency response.

As shown in Figure 7, both types of foam concentrates exhibited significant changes in appearance during the aging process. The color of AFFF gradually shifted from an initial clear light yellow to a turbid light brown. In addition, as shown in Figure 8, a small amount of precipitate appeared at the bottom of the concentrate after 32 days of aging, which may subsequently accumulate in pipelines. In comparison, the AFFF/AR displayed more drastic color changes. It deepened progressively from its original state to a brownish hue and eventually developed large areas of black regions, indicating that complex reactions might have occurred internally.

3.2 | Physicochemical properties variation analysis

Figure 9 presents the changes in basic physicochemical properties of aged foam concentrates. In terms of surface tension, both types of foam concentrates exhibited a continuous upward trend during the high-temperature accelerated aging. The AFFF increased from 16.738 to 17.249 mN/m, and the AFFF/AR from 16.687 to 17.260 mN/m, but the increases for both were no more than 4%. Considering the excellent thermal stability of the surfactants, no thermal decomposition occurred at 80°C. Therefore, the slight increase in surface tension was more likely caused by changes in the solution state rather than surfactant decomposition. Elevated temperature reduced solution uniformity, and dissolved ions disturbed the interfacial arrangement of surfactant molecules. Together, these effects weakened surface activity.

Regarding pH values, the AFFF/AR showed an increase by 15.1%, while the AFFF increased by 6.9%. The corrosion of aluminum alloy led to significant changes in the hydrogen ion levels in the system, with the overall pH exhibiting an upward trend, indicating a relative increase in hydroxide ion concentration. At the same time, the growth in ion concentration also drove drastic changes in conductivity. The AFFF/AR increased by 13.4 times, and the AFFF by 8.1 times, further proving the reaction between the concentrate and the alloy as well as a substantial rise in the number of ions. In terms of viscosity changes, the two formulations exhibited completely different aging behaviors. The viscosity of AFFF fluctuated within a certain range, with relatively mild variations. In contrast, the viscosity of AFFF/AR sharply rose from 118.86 to 452.553 mPa·s at 32 days of aging, and subsequently, due to the transformation into a gel state in the later stages of aging, its parameters could no longer be measured using a rotational viscometer.

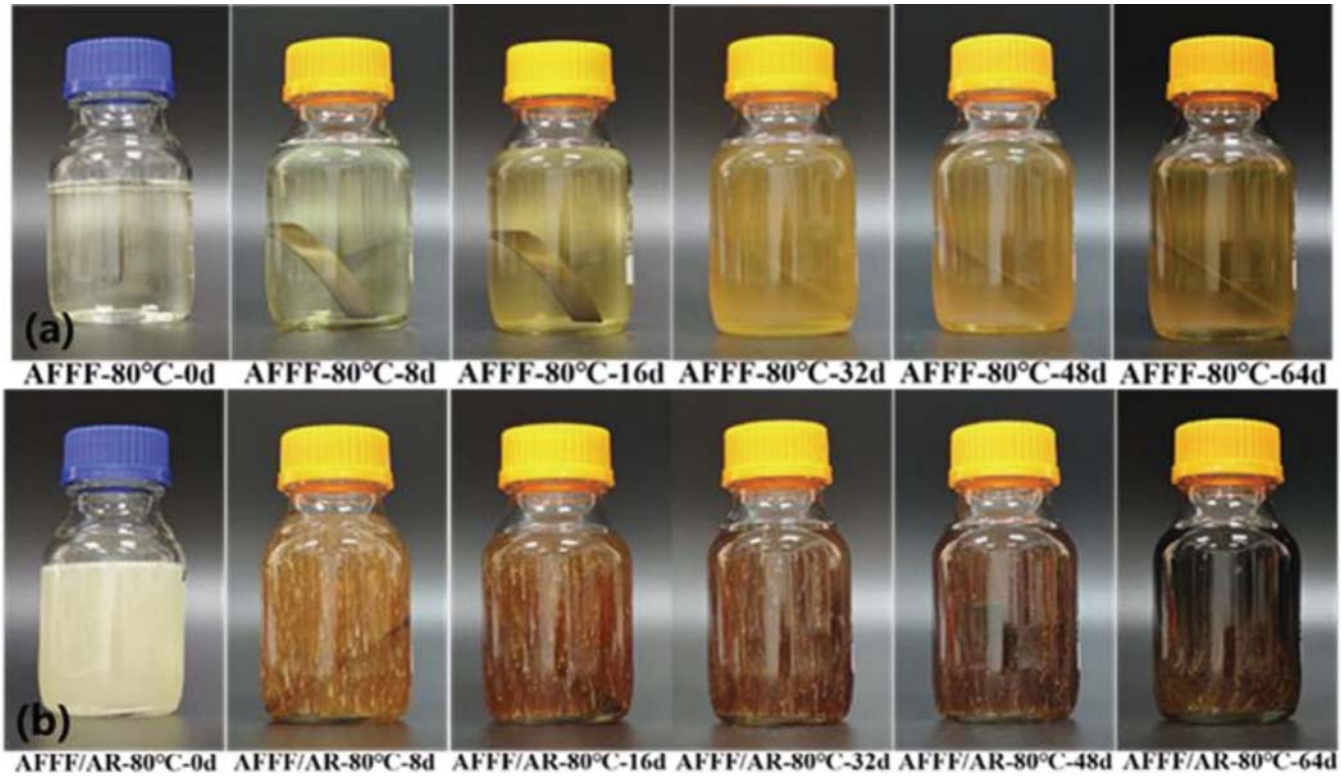

FIGURE 7 Variation of foam concentrate with processing time (A) AFFF (B) AFFF/AR.

3.3 | Analysis of the mechanism governing concentrate changes

It is noteworthy that during the aging process of the AFFF/AR concentrate, not only did its color change, but its physical form also transformed. As shown in Figure 10, the AFFF/AR gradually transitioned from a viscous liquid to a gel-like state as the aging time increased. At this stage, the concentrate had essentially lost its fluidity and presented an overall jelly-like appearance, accompanied by a pronounced ammonia odor. This phenomenon became more evident with further aging.[16]

Molecular dynamics simulation also revealed this phenomenon. Mean squared displacement (MSD) refers to the average displacement of particles relative to their initial positions over a given time interval. In general, MSD increases approximately linearly with time, and the diffusion coefficient can be determined from its growth rate to quantify the mass-transport capability of molecules.[17] As shown in Figure 11, the mobility of water molecules was markedly suppressed in the system with Al^{3+}. The MSD decreased from 1.0068 to 0.868, representing a reduction of 13.8%. The weakened diffusion capability of water molecules suggests that the internal environment of the concentrate tends to become more restricted. This change at the microscopic level aligns with the gelation phenomena observed in experiments. Furthermore, the dynamic constraining effect of Al^{3+} on the XG molecular chains was even more pronounced. In the aluminum-containing system, the MSD curve of XG exhibited a typical plateau region, which is a characteristic feature of hindered chain

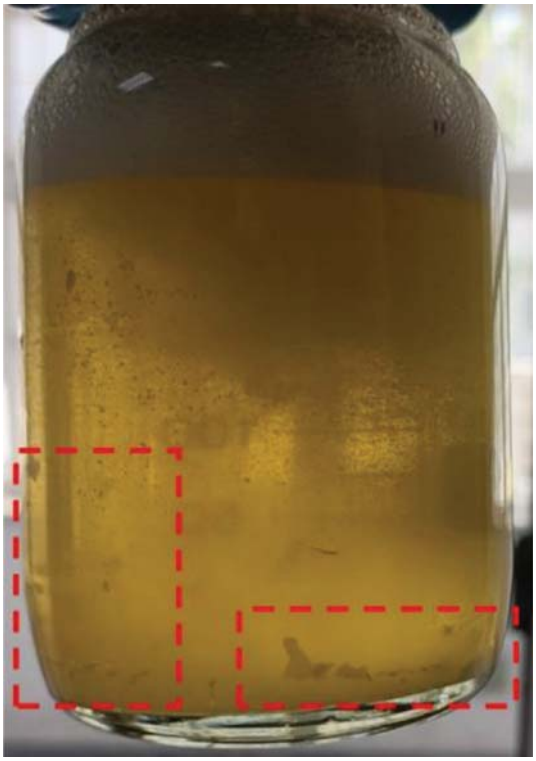

FIGURE 8 Flake-like precipitates in the AFFF system aged for 64 days.

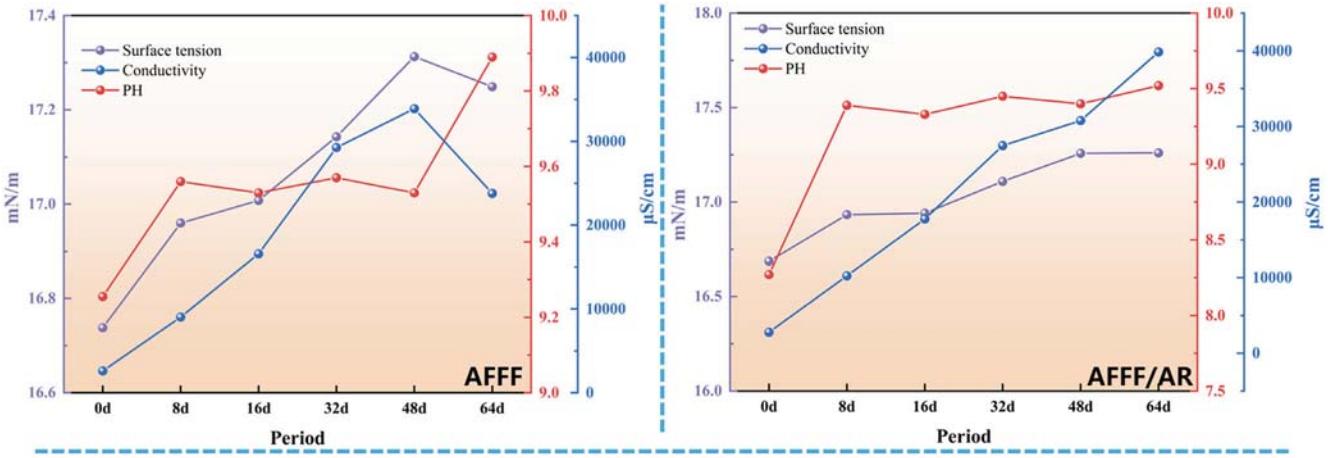

Viscosity/mPa·s						
	0d	8d	16d	32d	48d	64d
AFFF	3.272	3.757	4.180	3.940	3.875	4.133
AFFF/AR	118.86	155.432	291.549	452.553	/	/

FIGURE 9 Curve of physical and chemical properties.

FIGURE 10 Morphological features of the gel.

segment motion and the system entering a state of dynamic stagnation. In contrast, the MSD curve in the system without aluminum ions remains steadily increasing. This pronounced kinetic disparity confirms that trivalent aluminum ions effectively constrain the available space for molecular motion. However, the specific mechanism of gelation still requires further analysis and discussion.

3.3.1 | System energy variation analysis

Energy analysis can directly reveal the system state and reflect the form of strong intermolecular interactions. The total potential energy is defined as the sum of all potential energy terms in the force field. Under the same conditions, a lower average total potential energy usually indicates stronger intermolecular interactions and a thermodynamically more favorable configuration.[18,19] As shown in Figure 12, the total energy of the AC1 system decreased by 61613.059 kcal/mol compared to AC2. This indicates that the introduced aluminum ions have stabilized the XG molecular system through a stronger intermolecular attractive force. At the same time, the results show that the aluminum ions significantly enhanced the electrostatic interactions in the system, with the electrostatic energy in the AC1 system declining by 70468.322 kcal/mol relative to the AC2 system. In the concentrate, the aluminum ions carry a strong positive charge, while each xanthan monomer carries two negative charges. Therefore, there will be a significant electrostatic attraction between them, causing the aluminum ions to cluster near the carboxyl groups of xanthan. At the same time, in this charged system, non-covalent interactions are mainly dominated by the electrostatic term. The enhancement of electrostatic attraction will cause the overall non-covalent energy to shift toward a more negative value. Furthermore, the change in bond energy reflects the increase in the internal conformational tension of the molecule. This indicates that under the influence of aluminum ions, the xanthan chain deviates from its equilibrium geometric configuration, which is consistent with the experimental results presented later.

3.3.2 | Radial distribution function and coordination number analysis

The radial distribution function (RDF) and coordination number (CN) are widely used to characterize the local coordination environment between interacting species.[20–22] Taking Al^{3+} as the reference center, the experiment calculated its relative distribution with respect to carboxylate groups and water molecules, as shown in Figure 13.

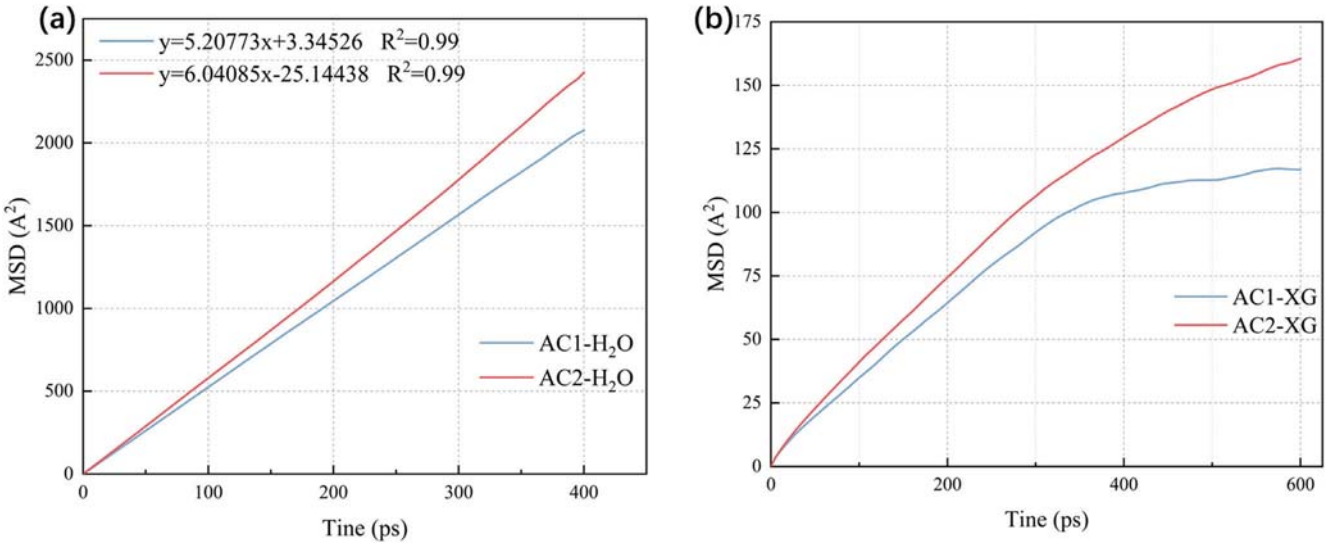

FIGURE 11 The curve of MSD: (A) H_2O (B) XG.

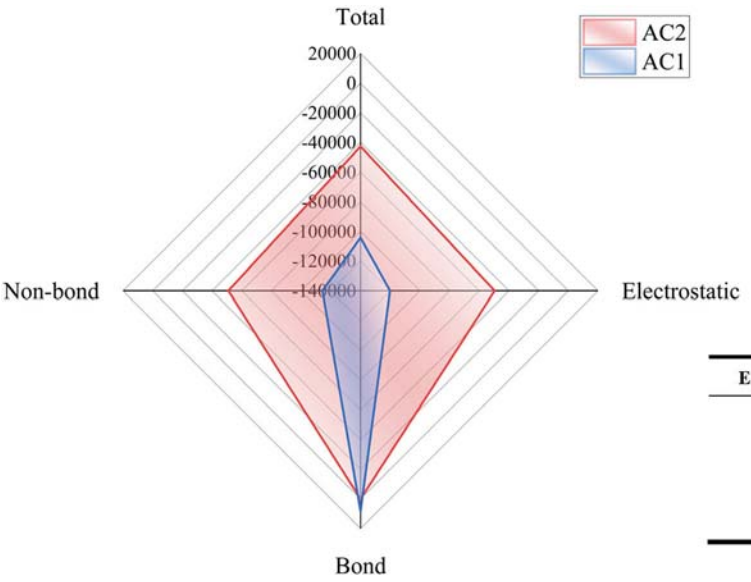

Energy/(kcal/mol)	AC1	AC2
Total	-04256.984	-2643.925
Electrostatic	-20193.148	-9724.816
Bond	8255.426	6551.902
Non-bond	-14364.677	-0986.603

FIGURE 12 Energy distribution of the system.

For Al^{3+}–carboxylate coordination, a sharp primary peak appears at $r \approx 2.57$ Å with $g(r) \approx 19.99$. A secondary peak is also observed at $r \approx 2.63$ Å with $g(r) \approx 18.69$. At the boundary of the first coordination layer, the CN is 0.1, indicating that on average each Al^{3+} forms a bridge with only a small number of carboxylic oxygen groups. In contrast, Al^{3+}–water exhibits a broader peak at $r \approx 2.63$ Å, followed by a decay toward a minimum. The CN is approximately 3 at $r = 2.63$ Å and increases to about 7 at the end of the first hydration shell, indicating that Al^{3+} is strongly solvated in the surrounding environment.

The gelation phenomenon observed in the experiments is driven by coordination bridging between Al^{3+} and xanthan.[23–25] Such bridging promotes the development of a denser three-dimensional network. In addition, electrostatic attraction facilitates chain association and aggregation. Coordination sites on xanthan are limited, so an excess of Al^{3+} leads to a low average CN for Al^{3+}–COO^-. This low CN can be further amplified by restricted site accessibility and competitive hydration by water. Although the first-shell CN of Al^{3+}–COO^- is small, the extremely high near-contact $g(r)$ indicates strong and specific binding once contact is established. This behavior also suggests that the gelation process is difficult to reverse. Once strong coordination and electrostatic interactions are established between aluminum ions and XG, simple dilution cannot readily restore the original fluid state. This is unfavorable for the long-term storage and emergency readiness of fire suppression systems.

3.3.3 | Conformational evolution of XG

The radius of gyration is an important parameter for characterizing the overall conformational evolution of polymer chains and

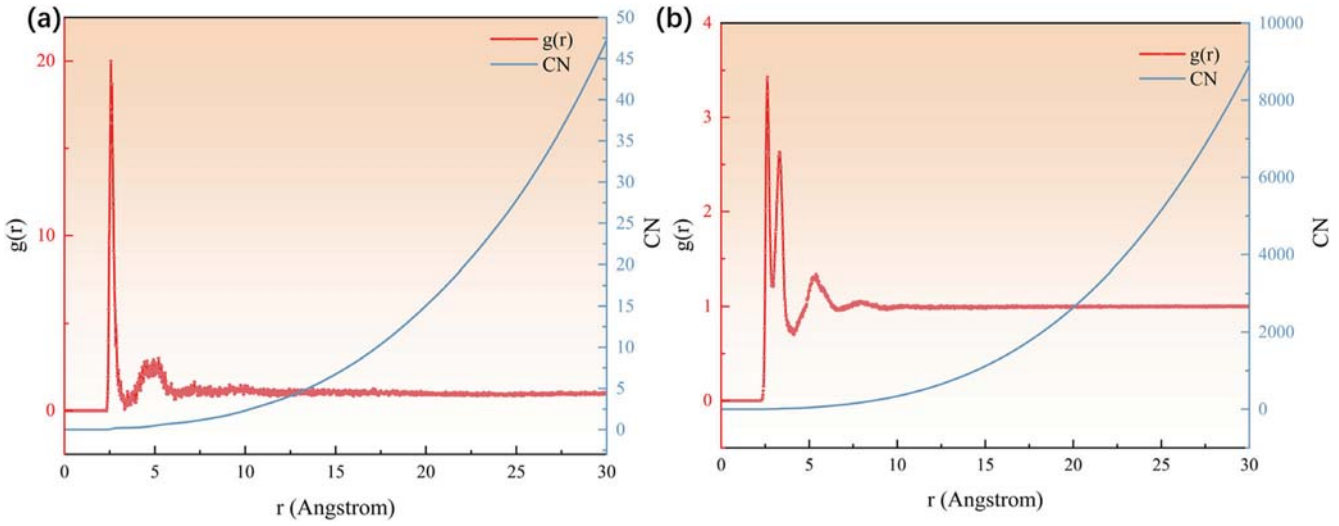

FIGURE 13 Radial distribution function and coordination number: (A) Coordination between Al^{3+} and COO^{-} (B) Coordination between Al^{3+} and H_2O.

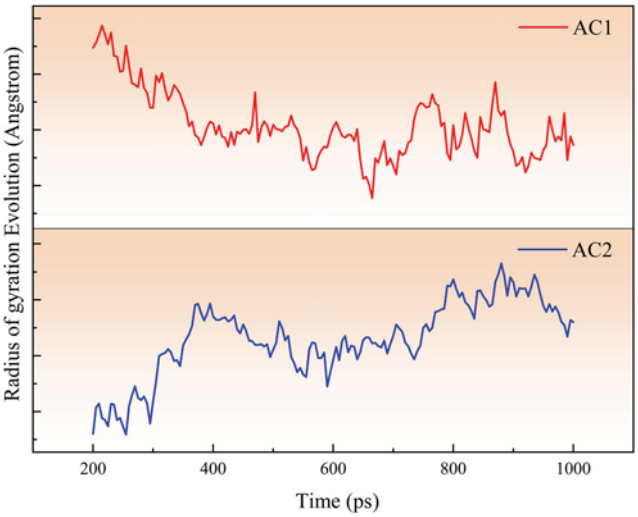

FIGURE 14 Variation in the radius of gyration with time.

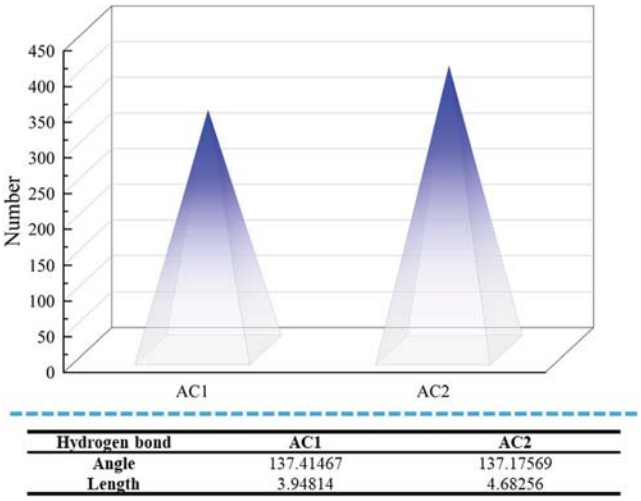

Hydrogen bond	AC1	AC2
Angle	137.41467	137.17569
Length	3.94814	4.68256

FIGURE 15 Hydrogen bonding information of the system.

can be used to determine whether the chains undergo contraction or relaxation. As shown in Figure 14, the introduction of Al^{3+} exerted a measurable influence on the conformational evolution of XG molecules. In the aluminum-free system, the radius of gyration continuously increased, with the polymer molecular chains gradually relaxing in the concentrate. In the aluminum-containing system, the radius of gyration displayed a continuous downward trend. The coordination bridging and electrostatic attraction between Al^{3+} and XG jointly drive this behavior. The continuous decrease in the radius of gyration indicates restricted segmental mobility, suggesting the progressive formation of a network-like structure within the system, which in turn leads to an extreme increase in viscosity.

3.3.4 | Hydrogen bonding network evolution and interaction analysis

Hydrogen-bond analysis is used to evaluate changes in the solvation structure and to reveal whether the interactions between water molecules and polymer functional groups are competitively affected or reconstructed by ions. As shown in Figure 15, the hydrogen-bonding characteristics between carboxylate oxygen atoms and water molecules are presented. The average number of hydrogen bonds formed between carboxylate groups and water decreases from 397.8308 to 335.7463, corresponding to a reduction of approximately 15.6%. This indicates that the connectivity between carboxylates and water is weakened in the presence of Al^{3+}. However, the hydrogen-bond geometry remains nearly unchanged.

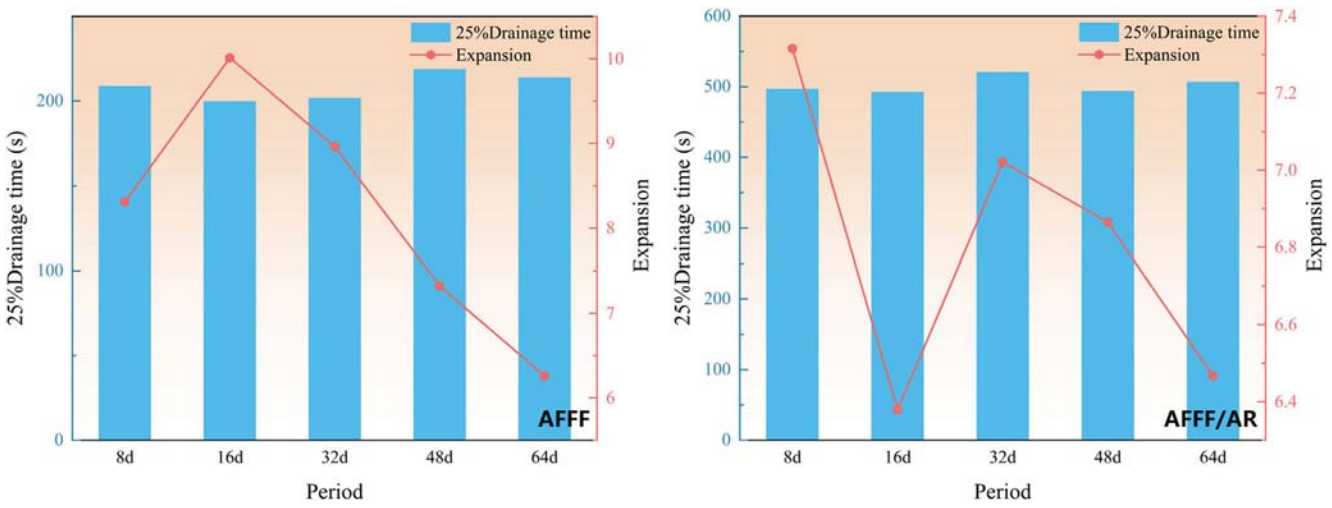

FIGURE 16 The variation of foam performance with the aging period.

Together, these results suggest that Al^{3+} primarily reduces the number of hydrogen bonds between carboxylates and water, rather than markedly altering the typical geometric features of individual hydrogen bonds.

3.4 | Comparative analysis of fire extinguishing performance

3.4.1 | Foaming behavior and drainage characteristics

Foam concentrate usually needs to be mixed with water before use. For the concentrated liquid that has already become gel-like, experiments have found that it is difficult for it to dissolve with water to form an effective fire extinguishing agent. To evaluate its foaming performance, the sample was homogenized by prolonged high-speed stirring and then allowed to stand before testing. However, complete dissolution of the gel particles in water could not be ensured. As shown in Figure 16, the 25% drainage time for both samples remained relatively stable, even exhibiting a slight increase. This is because metal ions can form a hydration shell, which binds water molecules and reduces their mobility in the foam films. In addition, metal ions screen charges and decrease the electrostatic repulsion between surfactant head groups, thereby enhancing foam stability. Although the foam expansion ratio showed some fluctuations, it generally showed a significant downward trend. The decline amplitudes reached up to 37.46% and 12.84%. And the AFFF exhibited a more pronounced degradation phenomenon. This indicates that in the AFFF/AR solution after uniform stirring, XG plays a certain role in foam stabilization to resist the damage caused by aging to the solution.[23,24]

3.4.2 | Effectiveness of fire suppression system

A foam fire suppression system is considered effective and reliable only when foam with fire extinguishing capability can flow through the pipeline under pressure and be discharged successfully. The flowability of the foam is closely associated with its viscosity. When the viscosity increases, the fluidity of foam decreases markedly, thereby weakening or even losing its ability to be effectively discharged and to extinguish fires. Under steady state, incompressible, and fully developed flow in a circular tube, the apparent wall shear rate can be expressed by Equation (3). The relationships among the apparent viscosity and the wall shear stress are given in Equations (4) and (5). By combining these equations, the relationship between the pressure drop in the tube and the viscosity can be derived, as shown in Equation (6).

$$\dot{\gamma}_{app} = \left(\frac{3n+1}{4n}\right)\frac{8v}{D} = \left(\frac{3n+1}{4n}\right)\frac{32Q}{\pi D^3} \tag{3}$$

$$\eta_{app} = \frac{\tau_w}{\dot{\gamma}_{app}} \tag{4}$$

$$\tau_w = \frac{\Delta P D}{4L} \tag{5}$$

$$\Delta P = \left(\frac{3n+1}{4n}\right)\frac{32\eta_{app}Lv}{D^2} = \left(\frac{3n+1}{4n}\right)\frac{128\eta_{app}QL}{\pi D^4} \tag{6}$$

Here, $\dot{\gamma}_{app}$ denotes the apparent wall shear rate; η_{app} is the apparent viscosity; τ_w is the wall shear stress; ΔP represents the pressure drop; v is the mean velocity in the tube; Q is the volumetric flow rate; $\mathcal{D}$ is the inner diameter of the tube; L is the tube length; n is the flow behavior index. Prolonged direct contact with the alloy results in a pronounced increase in viscosity. According to Equation (6), the elevated viscosity correspondingly leads to a dramatic increase in the pressure drop along the pipeline. Moreover, the intensified pressure loss gives rise to operational anomalies, including restricted discharge and an inability to maintain a stable and continuous foam spray. Once the pressure drop exceeds a critical limit, the foam concentrate can no longer sustain flow within the tube. The aged AFFF/AR concentrate

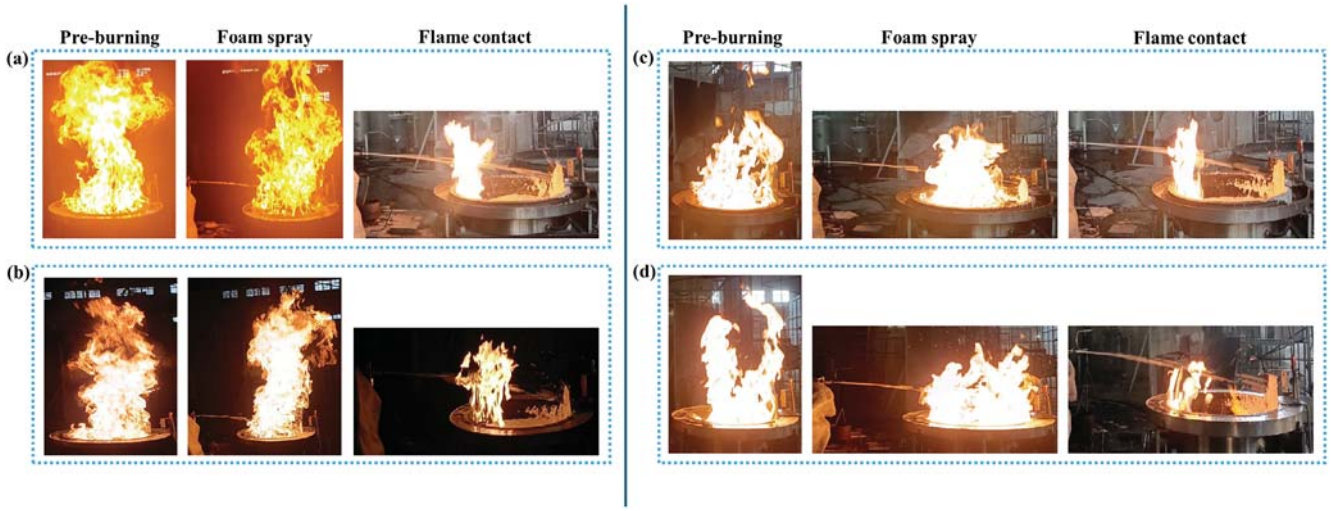

FIGURE 17 Representative fire extinguishing stages. (A) AFFF-0d; (B) AFFF-32d; (C) AFFF/AR-0d; (D) AFFF/AR-32d.

TABLE 2 Fire extinguishing parameters.

Medium	Fuel	Injection method	Fire extinguishing time
AFFF-0d	Gasoline	Gentle application	31″36
AFFF-32d			33″10
AFFF/AR-0d	Ethyl alcohol	Gentle application	3′24″02
AFFF/AR-32d			3′56″72

corresponds to this situation, as it has essentially lost its ability to flow through the pipeline and to effectively extinguish fires.

To clarify the actual fire suppression efficiency of aged foam and compare the aging effects on samples, fire suppression experiments were conducted as shown in Figure 17. Based on the experimental results, fire suppression tests were conducted using foam concentrates aged for 32 days and compared against unaged (0 day) samples. The experiments employed a positive pressure foaming system and scaled-down oil pans to simulate realistic fire scenarios; the device is shown in Figure 2. As shown in Table 2, both foam solutions exhibited a clear decline in fire suppression efficiency. The extinguishing time of AFFF increased by 5.5%, while that of AFFF/AR increased by 16%. Combined with the observed reduction in foam expansion, these results indicate that the foam layer after aging became thinner and less stable, which reduced the surface coverage area and weakened the ability to isolate oxygen. As a result, the suppression efficiency of the foam system decreased under the same fire conditions. Moreover, the more severe deterioration observed in the AFFF/AR system suggests that the cross linking between XG and metal ions reduced the ability of the solution to resist dissolution by polar liquids.

In summary, the multiple uncertainties associated with storage tank corrosion and foam agent aging can significantly reduce the operability and discharge capacity of the extinguishing agent. As a result, the foam fire suppression system may fail to deliver a stable output under emergency conditions, thereby weakening system reliability and increasing process safety risks.

4 | CONCLUSION

This study investigated the storage stability and performance evolution patterns of AFFF extinguishing agents in aluminum alloy containers through a high-temperature accelerated aging test system, and employed molecular dynamics simulation to reveal the intrinsic mechanisms of performance degradation from a microscopic scale. The main conclusions are as follows:

1. Corrosion of aluminum alloys can markedly degrade the performance of foam agents for fire suppression. Under accelerated aging at 80°C, the expansion ratios of AFFF and AFFF/AR decreased by 37.46% and 12.84%, while both pH and electrical conductivity increased substantially. After aging, the AFFF/AR formulation containing XG underwent severe gelation and further lost its flowability. In contrast, precipitation was observed in AFFF.
2. The simulation results indicate that the Al^{3+} ions released by corrosion will enhance electrostatic attraction and the coordination bridging effect with the carboxyl groups of xanthan gum. This ion-mediated cross-linking effect restricts the mobility of molecules and promotes the formation of the network, providing a mechanistic basis for the observed rheological transition.
3. Fire suppression tests indicate that aging leads to a moderate decline in extinguishing efficiency, whereas the formation of gels and precipitates severely impairs the operability of the system. Such corrosion-induced aging introduces latent failure modes that

compromise the reliability and process safety of foam fire suppression systems.

AUTHOR CONTRIBUTIONS

Zhengyang Wang: Investigation. **Wei Wang:** Investigation. **Peiyao Chen:** Methodology. **Lichen Zhang:** Methodology. **Liming Hu:** Data curation. **Xikang Zhang:** Data curation. **Qihang Yue:** Writing – original draft; conceptualization; formal analysis. **Biao Zhou:** Writing – review and editing; supervision; validation. **Kai Wang:** Writing – review and editing; supervision; validation.

ACKNOWLEDGMENTS

This work was supported by the Ordos Key Research and Development Program (No. YF20240026), Beijing Nova Program (No. 202504841008), the Key-Area Research and Development Program of Guangdong Province (No. 2024B1111080002), and the Fundamental Research Funds for the Central Universities (No. 2025ZKPYAQ03), Natural Science Foundation of Shanghai (No. 24ZR1473000, No. 25ZR1402516).

CONFLICT OF INTEREST STATEMENT

The authors declared that they have no conflicts of interest for this work. We declare that we do not have any commercial or associative interest that represents a conflict of interest in connection with the work submitted.

DATA AVAILABILITY STATEMENT

The data that support the findings of this study are available from the corresponding author upon reasonable request.

ORCID

Wei Wang https://orcid.org/0000-0002-5401-4067
Biao Zhou https://orcid.org/0000-0003-3517-699X

REFERENCES

1. Wang Z, Jiang X, Yang C, Zhou B. Experimental study on thermal stability and burn-back performance of aqueous film forming foam agent (AFFF) with short-chain fluorocarbon surfactant or flame retardant. *Fire Saf J*. 2024;146:104135. doi:10.1016/j.firesaf.2024.104135
2. Kong D, Wang D, Chen J, et al. Assessing the mixed foam stability of different foam extinguishing agents under room temperature and thermal radiation: An experimental study. *J Mol Liq*. 2023;369:120805. doi:10.1016/j.molliq.2022.120805
3. Wang Z, Xiao P, Yang J, et al. Micro-structure characteristics and the fire-extinguishing performance of aqueous film-forming foam mixed with short-chain fluorocarbon surfactant. *Phys Fluids*. 2025;37:017115. doi:10.1063/5.0244168
4. An Z, Liu Z, Ha H, Zhao T, Pan R, Zhou X. Study of the stability of alcohol-resistant aqueous film forming foam on class B fuels with different polarity and boiling point. *Case Stud Therm Eng*. 2025;72:106380. doi:10.1016/j.csite.2025.106380
5. Bao Y, Zhi H, Wang L. Rheological behavior of alcohol-resistant foam concentrates and its impact on pipe flows. *Fire Saf J*. 2021;121:103289. doi:10.1016/j.firesaf.2021.103289
6. Yang Y, Zou Y, Nie L, Shang F, Li K, Zhang J. Mechanism of Welan gum and silica nanoparticles on the foam properties and aggregation behavior of hydrocarbon and Gemini fluorocarbon surfactant dispersion. *Therm Sci Eng Progr*. 2025;59:103338. doi:10.1016/j.tsep.2025.103338
7. Zhang X, Bao Z, Fu X, Hu C, Jing L. Acute toxicity of aqueous film forming foam (AFFF) to zebrafish (*Brachydanio rerio*). *IOP Conf Ser Earth Environ Sci*. 2018;199:032010. doi:10.1088/1755-1315/199/3/032010
8. Patrascu MT, Busuioc AD, Busuioc C, et al. Experimental study on the corrosion of carbon steel and aluminum alloy in firefighting protein foam concentrates. *Materials*. 2021;14:7259. doi:10.3390/ma14237259
9. Rossi S, Eyraud M, Vacandio F, Massiani Y. Corrosivity of long-term fire retardant fire Trol® 931 and fire foam® 103 on aluminium alloys and steel. *Mater Chem Phys*. 2007;105:260-267. doi:10.1016/j.matchemphys.2007.04.055
10. Araujo LS, Mounzer EC, Wavrik JRA. Corrosion in fire protection systems in an offshore unit undergoing decommissioning. *Acta Sci Technol*. 2025;47:e71023. doi:10.4025/actascitechnol.v47i1.71023
11. Su P, Fuller DB. Corrosion and Corrosion Mitigation in Fire Protection Systems.
12. Jiang K, Kong D, Wang D. Study on the corrosion of metal of firefighting equipment by foam extinguishing agent at different temperatures. *Fire Sci Technol*. 2024;43:113-119.
13. Kostyaev AA, Balmasov AV, Inasaridze LN. Effect of inhibitors on carbon steel corrosion in foaming solutions. *Russ J Gen Chem*. 2016;86:429-433. doi:10.1134/S1070363216020420
14. Ye L, Kong D, Zhang J. Study on the effect of fluoroprotein foam extinguishing agent components on the corrosion of Q235 galvanized steel. *Fire Sci Technol*. 2025;44:230-235, 249. doi:10.20168/j.1009-0029.2025.02.0230.06
15. Sun T, Miao X, Jiang K, et al. Study on the impact of core components in Fluoroprotein foam fire extinguishing agents on the corrosion of aluminum alloys. *J Saf Environ*. 2024;24:4287-4295. doi:10.13637/j.issn.1009-6094.2024.0856
16. Marudova-Zsivanovits M, Jilov N, Gencheva E. Rheological investigation of xanthan gum–chromium gelation and its relation to enhanced oil recovery. *J Appl Polym Sci*. 2007;103:160-166. doi:10.1002/app.25025
17. Santo KP, Fabijanic KI, Cheng C-Y, Potanin A, Neimark AV. Modeling of the effects of metal complexation on the morphology and rheology of xanthan gum polysaccharide solutions. *Macromolecules*. 2021;54:8675-8692. doi:10.1021/acs.macromol.1c01328
18. Zarriz A, Journaux B, Powell-Palm MJ. On the equilibrium limit of liquid stability in pressurized aqueous systems. *Nat Commun*. 2024;15:10666. doi:10.1038/s41467-024-54625-z
19. Shmool TA, Martin LK, Matthews RP, Hallett JP. Ionic liquid-based strategy for predicting protein aggregation propensity and thermodynamic stability. *JACS Au*. 2022;2:2068-2080. doi:10.1021/jacsau.2c00356
20. Valente ÉC, Polêto MD, de Oliveira TV, et al. Effects of the cations Li+, Na+, K+, Mg2+, or Ca2+ on physicochemical properties of xanthan gum in aqueous medium – a view from computational molecular dynamics calculations. *Food Biophys*. 2023;18:32-47. doi:10.1007/s11483-022-09773-4
21. Ong EES, O'Byrne S, Liow J-L. Molecular dynamics study on the structural and dynamic properties of xanthan gum in a dilute solution under the effect of temperature. *AIP Conf Proc*. 2018;1954:030008.
22. Du L, Wang S, Zhang T, Xu C. Molecular dynamics simulation of the effect of calcium ions on the foamability of anionic surfactants. *Colloids Surf A Physicochem Eng Asp*. 2025;707:135819. doi:10.1016/j.colsurfa.2024.135819
23. Nolte H, John S, Smidsrød O, Stokke BT. Gelation of xanthan with trivalent metal ions. *Carbohydr Polym*. 1992;18:243-251. doi:10.1016/0144-8617(92)90089-9

24. Rodd AB, Cooper-White J, Dunstan DE, Boger DV. Gel point studies for chemically modified biopolymer networks using small amplitude oscillatory rheometry. *Polymer*. 2001;42:185-198. doi:10.1016/S0032-3861(00)00311-6
25. Gioia F, Ciriello PP. The containment of oil spills in porous media using xanthan/aluminum solutions, gelled by gaseous CO_2 or by $AlCl_3$ solutions. *J Hazard Mater*. 2006;138:500-506. doi:10.1016/j.jhazmat.2006.05.095

How to cite this article: Wang K, Yue Q, Chen P, et al. Impact of metal corrosion on the process safety of foam fire suppression system. *Process Saf Prog*. 2026;1-13. doi:10.1002/prs.70066